Kinetics of 5α-Cholestan-3β-yl *N*-(2-Naphthyl)carbamate/ *n*-Alkane Organogel Formation and Its Influence on the Fibrillar Networks

Xiao Huang,[†] Pierre Terech,[‡] Srinivasa R. Raghavan,[§] and Richard G. Weiss*,[†]

Contribution from the Department of Chemistry, Georgetown University, 37th and O Streets, NW, Washington, D.C. 20057-1227, CEA-UMR5819, Laboratoire Physico-Chimie Moléculaire, 17 rue des Martyrs, 38054 Grenoble Cedex 9, France, and Department of Chemical Engineering, University of Maryland, College Park, Maryland 20742-2111

Received December 7, 2004; E-mail: weissr@georgetown.edu

Abstract: The kinetics and mode of nucleation and growth of fibers by 5α-cholestan-3β-yl *N*-(2-naphthyl)-carbamate (**CNC**), a low-molecular-mass organogelator (LMOG), in *n*-octane and *n*-dodecane have been investigated as their sols were transformed isothermally to organogels. The kinetics has been followed in detail by circular dichroism, fluorescence, small-angle neutron scattering, and rheological methods. When treated according to Avrami theory, kinetic data from the four methods are self-consistent and describe a gelation process involving one-dimensional growth and "instantaneous nucleation". As expected from this growth model, polarized optical micrographs of the self-assembled fibrillar networks (SAFINs) show fibrous aggregates. However, their size and appearance change abruptly from spherulitic to rodlike as temperature is increased. This morphological change is attended by corresponding excursions in static and kinetic CD, fluorescence and rheological data. Furthermore, the rheological measurements reveal an unusual linear increase in viscoelastic moduli in the initial stages of self-assembly. Each of the methods employed becomes sensitive to changes of the system at different stages of the transformation from single molecules of the LMOG to their eventual SAFINs. This study also provides a methodology for investigating aggregation phenomena of some other self-assembling systems, including those of biological and physiological importance.

Introduction

A great deal of effort has been expended to develop new types of low-molecular-mass organogelators (LMOGs) and to understand the links between the properties and structures of LMOGs and their organogels.[1,2,3] Factors associated with the kinetics of *bulk* crystallization from melts or solutions have also been investigated carefully.[4] However, very few detailed studies related to the kinetics of molecular gel formation have been reported.[5] Here, we investigate the kinetics of formation of

organogels comprised of 5α-cholestan-3β-yl *N*-(2-naphthyl)-carbamate (**CNC**), one of the so-called ALS (*a*romatic *l*inker *s*teroid) class of organogelators,[6] and two *n*-alkanes as the liquid using four techniques—circular dichroism (CD), small-angle neutron scattering (SANS), rheology, and fluorescence—that probe different aspects of the aggregation process and become sensitive to them at different stages of aggregation. The kinetic data sets have been treated according to a statistical model based upon Avrami theory.[5,7] Furthermore, the structures of the self-assembled fibrillar networks (SAFINs) of the gels and a very interesting temperature-related morphological transition, from spherulitic to rodlike aggregates, are reported. To the best of our knowledge, this is the most comprehensive and instructive kinetic investigation related to molecular gels.

CNC
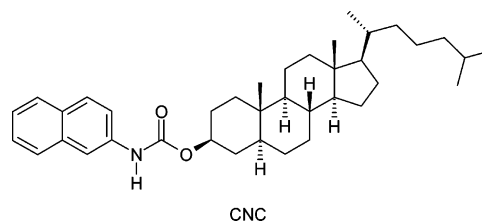
Molecular gels, especially organogels, have received a great deal of attention during the past few years due to their relevance to nanoscience and self-assembly. They are comprised of small

† Georgetown University.
‡ CEA-Grenoble.
§ University of Maryland.

(1) (a) George, M.; Weiss, R. G. *J. Am. Chem. Soc.* **2001**, *123*, 10393−10394. (b) George, M.; Snyder, S. L.; Terech, P.; Glinka, C. J.; Weiss, R. G. *J. Am. Chem. Soc.* **2003**, *125*, 10275−10283. (c) Jung, J. H.; John, G.; Masuda, M.; Yoshida, K.; Shinkai, S.; Shimizu, T. *Langmuir* **2001**, *17*, 7229−7232. (d) Friggeri, A.; Gronwald, O.; van Bommel, K. J. C.; Shinkai, S.; Reinhoudt, D. N. *J. Am. Chem. Soc.* **2002**, *124*, 10754−10758. (e) van Esch, J. H.; Feringa, B. L. *Angew. Chem., Int. Ed.* **2000**, *39*, 2263−2266.
(2) Weiss, R. G., Terech, P., Eds. *Molecular Gels. Materials with Self-Assembled Fibrillar Networks*; Springer: New York, planned publication 2005.
(3) (a) Terech, P.; Weiss, R. G. *Chem. Rev.* **1997**, *97*, 3133−3159. (b) Abdallah, D. J.; Weiss, R. G. *Adv. Mater.* **2000**, *12*, 1237−1247.
(4) See for instance: (a) Davey, R. J.; Garside, J. *From Molecules to Crystallizers*, Oxford University Press: New York, 2000 and references therein. (b) Wunderlich, B., Ed. *Macromolecular Physics. Crystal Nucleation, Growth, Annealing*; Academic Press: New York, 1976; Vol. 2.
(5) (a) Terech, P. *J. Colloid Interface Sci.* **1985**, *107*, 244−255. (b) Liu, X. Y.; Sawant, P. D. *Adv. Mater.* **2002**, *14*, 421−426; (c) Liu, X. Y.; Sawant, P. D. *Appl. Phys. Lett.,* **2001**, *19*, 3518−3520.
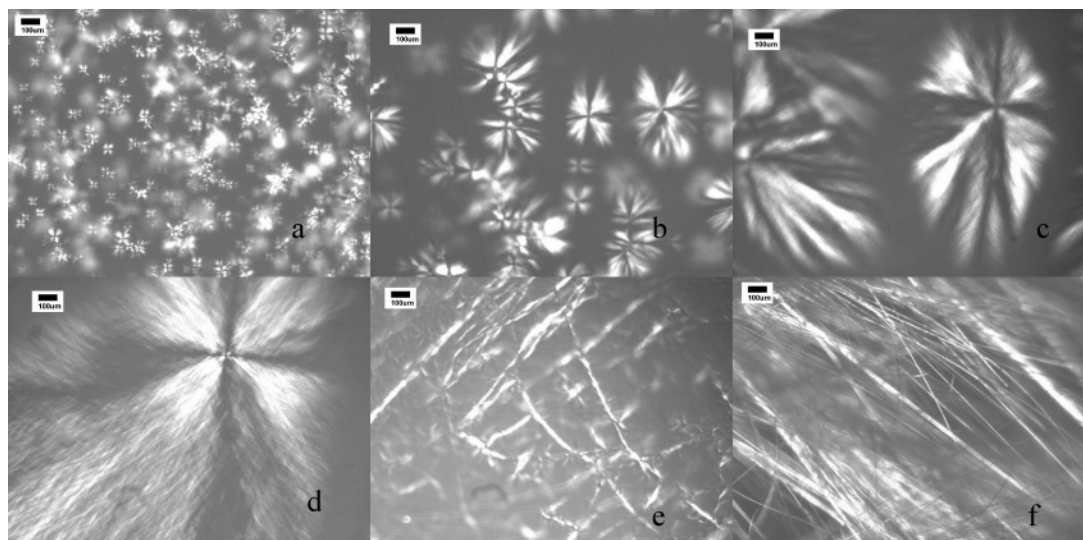
Figure 1. Optical micrographs of 1.0 wt % **CNC**/*n*-octane gels formed upon thermostating sols at (a) 0.0, (b) 15.6, (c) 25.1, (d) 31.6, (e) 37.4, and (f) 42.3 °C. The sample at 42.3 °C is not a gel.

amounts (usually ≤2 wt %) of an LMOG and an organic liquid.[3] Unlike many other forms of physical gels, they are usually thermally reversible. The LMOGs develop SAFINs that entrap the liquid components and stop macroscopic flow due to surface tension and capillary forces.[8] The fiber components of the SAFINs are stabilized by noncovalent intermolecular interactions that can be any (or a combination) of H-bonding, electrostatic attractions, and van der Waals forces.

Studies of molecular gel formation are more complex than those dealing with polymer gels because the latter start from a point at which one-dimensional self-assembled structures, polymeric chains, already exist.[9] Molecular gels require formation of one-dimensional, rodlike species (fibers, tapes, rods, etc.) as a first step in the self-assembly process leading to three-dimenional networks. On the other hand, nucleation and growth phenomena similar to those described here have been observed in several biologically and physiologically relevant systems whose components are structurally much more complex than ours. They include gelation via fibrous or spherulitic growth that depends on the degree of supersaturation in the deoxy state of sickle cell anemia hemoglobin,[10] fibrous gelation of insulin,[11] formation of long fibers[12a,b] or spherulitic-like bundles of fibrils of amyloid deposits with structurally disorganized centers in Alzheimer's disease plaques,[12c] filaments of actin,[13] fibrinogen,[14] tubulin,[15] and keratin,[16] and even disruption of the helical trimers

of collagen fibers under physiological conditions[17] (as well as their formation of gels when fully denatured[18]). The kinetics of the development of these systems is difficult to interpret due to the conformational complexity of the constituents and the myriad of intermolecular interaction pathways that are available to them. The **CNC**/*n*-alkane gelation system is much more tractable structurally and, as we demonstrate here, kinetically. As such, it may serve as a model for determining kinetic parameters (and relating them to structural growth patterns of aggregates) of the more complex systems.

Results and Discussion

Gelation of *n*-Alkanes by CNC. Results from a comprehensive survey of the gelation properties of **CNC** in several liquids, as well as those of structurally related LMOGs, have been reported.[6a] When cooled, sols of 0.9–3.0 wt % **CNC** in two *n*-alkanes, *n*-octane and *n*-dodecane, yielded translucent or opaque gels that were stable at room temperature for <1 day to >6 months, depending on the cooling protocol and LMOG concentration (Supporting Information Table 1). However, there is no clear relationship between the ranges of the characteristic temperatures at which gels form (gelation temperatures, T_g[19]) and the cooling protocol, but T_g does increase with **CNC** concentration.

SAFIN Structures from Optical Micrographs. Figure 1 shows optical micrographs of 1.0 wt % **CNC**/*n*-octane gels

(6) (a) Lu, L.; Cocker, M.; Bachman, R. E.; Weiss, R. G. *Langmuir* **2000**, *16*, 20–34. (b) Lin, Y.-C.; Kachar, B.; Weiss, R. G. *J. Am. Chem. Soc.* **1989**, *111*, 5542–5551.
(7) (a) Avrami, M. *J. Chem. Phys.* **1939**, *7*, 1103–1112. (b) Avrami, M. *J. Chem. Phys.* **1940**, *8*, 212–224.
(8) Terech, P.; Furman, I.; Weiss, R. G. *J. Phys. Chem.* **1995**, *99*, 9558–9566.
(9) Russo, P. S., Ed. *Reversible Polymeric gels and related system*; American Chemical Society: Washington, 1987.
(10) Galkin, O.; Vekilov, P. G. *J. Mol. Biol.* **2004**, *336*, 43–59.
(11) (a) Waugh, D. F. *J. Am. Chem. Soc.* **1946**, *68*, 247–250. (b) Jiminez, J. L.; Nettleton, E. J.; Bouchard, M.; Robinson, C. V.; Dobson, C. M. *Proc. Natl. Acad. Sci. U.S.A.* **2002**, *99*, 9196–9201.
(12) (a) Koo, E. H.; Lansbury, P. T., Jr.; Kelly, J. W. *Proc. Natl. Acad. Sci. U.S.A.* **1999**, *96*, 9989–9990. (b) Nilsson, *Methods* **2004**, *34*, 151–160. (c) Jin, L.-W.; Claborn, K. A.; Kurimoto, M.; Geday, M. A.; Maezawa, I.; Sohraby, F.; Estrada, M.; Kaminsky, W.; Kahr, B. *Proc. Natl. Acad. Sci. U.S.A.* **2003**, *100*, 15294–15298.
(13) (a) Ivkov, R.; Forbes, J. G.; Greer, S. C. *J. Chem. Phys.* **1998**, *108*, 5599–5607. (b) Greer, S. C. *Annu. Rev. Phys. Chem.* **2002**, *53*, 173–200.
(14) (a) Drukman, S.; Kavallaris, M. *Int. J. Oncol.* **2002**, *21*, 621–628. (b) Reinhart, W. H. *Biorheology* **2001**, *38*, 203–212.

(15) (a) Tuszynski, J. A.; Brown, J. A.; Sept, D. *J. Biol. Phys.* **2003**, *29*, 401–428. (b) Oakley, B. R.; Akkari, Y. N. *Cell Struct. Funct.* **1999**, *24*, 365–372.
(16) (a) Fuchs, E. *Annu. Rev. Cell Dev. Biol.* **1995**, *11*, 123–153. (b) Smack, D. P.; Korge, B. P.; James, W. D. *J. Am. Acad. Dermatol.* **1994**, *30*, 85–102.
(17) Leikina, E.; Mertts, M. V.; Kuznetsova, N.; Leikin, S. *Proc. Natl. Acad. Sci. U.S.A.* **2002**, *99*, 1314–1318.
(18) (a) Caria, A.; Bixio, L.; Kostyuk, O.; Ruggiero, C. *IEEE Trans. Nanobiosci.* **2004**, *3*, 85–89. (b) Wallace, D. G.; Rosenblatt, J. *Adv. Drug Deliv. Rev.* **2003**, *55*, 1631–1639. (c) Djabourov, M.; Leblond, J. In *Reversible and Polymeric Gels and Related Systems*; Russo, P. S., Ed.; American Chemical Society: Washington, 1987; Chapter 14.
(19) Although the magnitudes and ratios of the elastic (G') and loss (G'') moduli from rheological measurements provide a much more reliable viscoelastic distinction between a viscous sol and a gel,[19a] the "inverse flow" method[19b] was used to obtain approximate gelation temperatures. (a) Almdal, K.; Dyre, J.; Hvidt, S.; Kramer, O. *Polym. Gels Networks* **1993**, *1*, 5–17. (b) Eldridge, J. E.; Ferry, J. D. *J. Phys. Chem.* **1954**, *58*, 992–995.

prepared by incubating sols at different temperatures below T_g. The sol incubated at 0 °C led to highly branched, small fibers in spherulitic (colloidal) aggregates. With increasing gelation temperature, spherulitic assemblies of the gel became elongated and the gel made at 37.4 °C consisted of nonspherulitic, long fibrous assemblies.[20] At 42.3 °C, the long fibers were even more prevalent but phase separation was observed because the parallel orientation of the fibers precludes network formation via junction zones.[3a] This morphological transition, from spherulitic to fibrous (rodlike) growth patterns, is manifested in measurements that follow the kinetics of gelation by other techniques (vide infra).

An accepted mechanism for formation of this type of organogel includes stochastic nucleation, growth of branched fibers from a nucleation center, and formation of the three-dimensional network based on entanglement or direct interaction of the fibers via junction zones. In general, the lower the incubation temperature (increasing the reduced gelation temperature, $T_g - T$, and the degree of supersaturation), the greater the concentration driving force for crystallization and the smaller and more numerous are the crystals,[21] the more branched and more entangled will be the fibers,[22] and the faster and more probable is gelation.[23] Gels formed at higher temperatures (i.e., lower reduced temperatures) persisted for longer periods when kept at room temperature and were qualitatively stronger (Supporting Information Table 1).

At ≥ 1.5 wt % **CNC**, *n*-octane gels remained spherulitic, regardless of the incubation temperature (Supporting Information Figure 1). However, the tendency toward rodlike structures clearly increases with increased incubation temperatures, even at the higher LMOG concentrations. Transition from spherulitic to fibrous growth is certainly precedented in other types of crystallization phenomena, and spherulites are favored if static heterogeneities (e.g., particles or dirt) or dynamic heterogeneities (e.g., from supersaturation, as indicated by $T_g - T$) are pronounced.[24] In our system, fiberlike gel networks form over a narrow range of temperatures and **CNC** concentrations.

Intrafibrillar Morphology by X-ray Diffraction (XRD). Figure 2 presents X-ray diffraction profiles of *n*-octane gels formed at 40 °C and of neat, solid **CNC**. With time, the spherulitic (colloidal-type) gels phase-separated into very long fibers whose diffraction pattern is the same as that of the neat powder. Although the molecular packing within the rodlike gel structures (incubation at 40 °C) appears to be like that in the neat solid, packing within the gel spherulites (incubation at 0 °C) does not (Supporting Information Figure 2).

Polymorphism in "bulk" crystallizations has been investigated extensively and the thermodynamic basis for it is well understood.[25] However, predicting when more than one morph will be observed has remained an elusive goal. Polymorphism within the SAFINs of LMOG gels with different liquid components
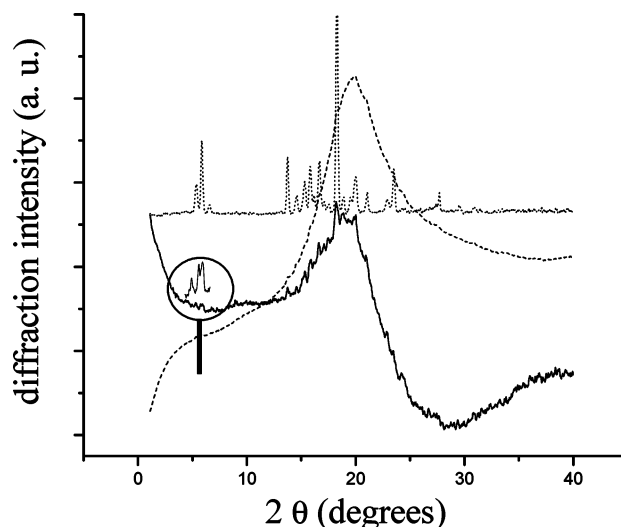

Figure 2. XRD patterns of a 3.0 wt % **CNC**/*n*-octane gel (incubation at 40.0 °C, - - -), gel diffraction with an empirical subtraction of the diffraction by neat *n*-octane (—), and the diffraction of neat solid **CNC** (···). The intensity of the circled part has been amplified.

or between a SAFIN and a "bulk" solid prepared within a nongelated liquid is not rare,[2,3] and it is well-documented for some of the other members of the ALS class besides **CNC**.[6] Different morphs of an ALS gel have been made even by changing the cooling protocol from one sol phase![26] The latter case appears to be operative here for **CNC**.

Kinetic Studies of CNC/*n*-Alkane Organogel Formation. (a) Kinetic Models and Data Treatments. The kinetics of nucleation and primary and secondary crystallization leading to macroscopic phase separations (i.e., "bulk" crystal growth) has been studied extensively in solutions and melts.[27] However, little is known about the kinetics of SAFIN formation in organogels. Most organogels form very rapidly once their sol phases are cooled to below T_g. Those comprised of **CNC** and one of several *n*-alkanes are transformed from sols to gels on a time scale of a few minutes to hours, depending on the temperature, allowing kinetic studies to be conducted conveniently. We have followed the transformations from sols to gels using four techniques that provide kinetic information based on different physical attributes of the system:

(1) Time-dependent SANS measurements provide information about changes of the sizes and numbers of scattering objects after stochastic nucleation commences.

(2) Time-dependent rheology follows the development of networks as the initially formed aggregates interact with each other.

(3) CD spectra of chiral **CNC**[6] open a window into the initial events within single aggregating objects because the CD intensities of helical aggregates can be much stronger than those of equal numbers of isolated molecules.[28]

(4) Fluorescence from naphthyl groups provides another monitor of the initial and subsequent stages of nucleation of **CNC** molecules because the spectral intensities and band shapes undergo significant changes as monomers merge into dimers and larger aggregates.

(20) Abe, H.; Kikuchi, H.; Hanabusa, K.; Kato, T.; Kajiyama, T. *Liq. Cryst.* **2003**, *12*, 1426−1431.
(21) Jones, R. A. L. *Soft Condensed Matter*; Oxford University Press: New York, 2002; Chapter 8.
(22) Lescanne, M.; Grondin, P.; d'Aléo, A.; Fages, F.; Pozzo, J.-L.; Mondain Monval, O.; Reinheimer, P.; Colin, A. *Langmuir* **2004**, *20*, 3032−3041.
(23) Abdallah, D. J.; Weiss, R. G. *Chem. Mater.* **2000**, *12*, 406−413.
(24) Gránásy, L.; Pusztai, T.; Börzsönyi, T.; Warren, J. A.; Douglas, J. F. *Nature Mater.* **2004**, *3*, 645−650.
(25) See for instance: (a) Verma, A. R.; Krishna, P. *Polymorphism and polytypism in crystals*; Wiley: New York, 1966. (b) Chapters 3 and 6 of ref 4.

(26) Furman, I.; Weiss, R. G. *Langmuir* **1993**, *9*, 2084−2088.
(27) See, for instance: Chapter 3 of ref 4 and references therein.
(28) (a) Ciferri, A. *Liq. Cryst.* **1999**, *26*, 489−494. (b) Brunsveld, L.; Vekemans, J. A. J. M.; Hirschberg, J. H. K. K.; Sijbesma, R. P.; Meijer, E. W. *Proc. Natl. Acad. Sci. U.S.A.* **2002**, *99*, 4977−4982.

A key question is, "What model should be used to treat the different sets of kinetic data?" The kinetic steps of a process are usually described either macroscopically (in terms of ensemble events that are characterized by rate constants and reaction orders) or microscopically (in terms of elementary probabilities and statistical models). Gelation of the sort described here is an inhomogeneous process in which a metastable, supercooled, macroscopically homogeneous (sol or solution) phase is transformed into a more stable (but frequently metastable), microscopically separated (gel) phase. During the transformation, the metastable and more stable phases may coexist, and the time course for the transformation may be governed by very complicated kinetic steps.[27] As a result, models that result in simple rate laws, such as those describing reactions of molecules in homogeneous media and involving transition states, are inappropriate. Although models based on stochastic events and probabilities are more appropriate, they are usually very difficult to apply rigorously. However, Avrami has developed equations to describe the crystallization of polymer melts[7] that can be applied to gelation processes.[5] Their application to our CD, SANS, fluorescence, and rheological data sets leads to mechanistic conclusions that are self-consistent both qualitatively and quantitatively.

Equations 1 and 2 are the same Avrami equation for crystallization and microscopic phase separation, but expressed in the exponential and log−log forms.[7]

$$1 - X = \exp(-Kt^{n}) \tag{1}$$

$$\ln\left(\ln\frac{1}{1-X}\right) = \ln K + n \ln t \tag{2}$$

As applied to gels, X is the volume fraction of the more stable phase (the gel in our case), K is a temperature-dependent parameter that is like a rate constant, n is the so-called Avrami exponent that reflects the type of growth leading to phase separation, and t is time. The Avrami exponent is temperature independent; its theoretical value (1, 2, 3, or 4, as well as half integers) is determined by the nature of the nucleation and crystal growth.[5,29] The development of these equations assumes that nucleation occurs either instantaneously (zero-order) or linearly (first-order) and that the small domains of the separated gel phase grow independently.

Other approaches, such as fractal[5b,c] and autocatalytic[5a] models, have also been employed to analyze kinetic data of this kind. For instance, the form of the equations from the fractal model is the same as that of Avrami except that the exponential factor is interpreted as a fractal dimension D_f instead of the branching behavior of the aggregates. Analyses of results based principally on the Avrami theory are presented here.

(b) Kinetic Data from Circular Dichroism. Due to the high optical densities below 300 nm of even dilute samples of **CNC**, only absorption features above 300 nm have been studied. Also, in dilute solutions (i.e., in the absence of aggregates), the large separation between the chiral cholestanyl part and the naphthyl chromophore of a **CNC** molecule results in a lack of perceptible CD intensity in the UV−vis region where the lowest energy naphthyl electronic absorptions occur (Figure 3). More con-

(29) (a) Schultz, J. M. *Polymer Materials Science*; Prentice Hall: Englewood Cliffs, NJ, 1974; p 385. (b) Wunderlich, B. *Macromolecular Physics*; Academic Press: New York, 1976; Vol 2, pp 16−52, 147.
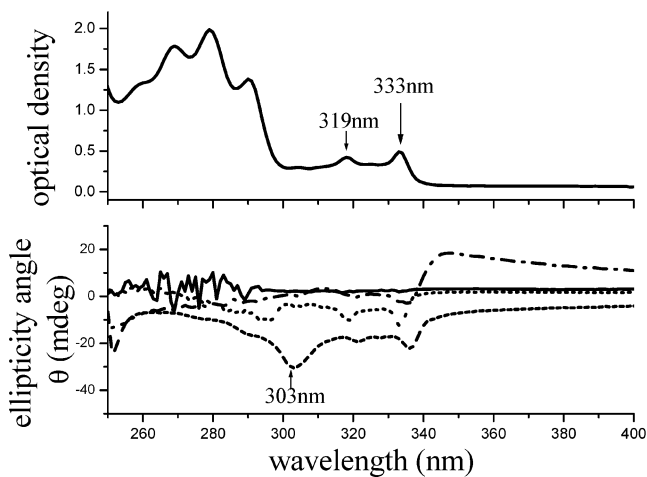
Figure 3. Spectra of **CNC**/*n*-octane samples at room temperature. Upper: UV−vis absorption spectrum of a 0.19 wt % **CNC** sol in a 1 cm path length cell. Lower: CD spectra of a 0.02 wt % **CNC** sol in a 5 cm path length cell (—), a 0.23 wt % **CNC** sol in a 5 mm path length cell (⋯), a 1.0 wt % **CNC** gel formed at 40.0 °C in a 1 mm path length cell (- - -), and 1.0 wt % **CNC** gel formed at 5.4 °C in a 1 mm path length cell (−·−).

centrated **CNC** solutions in *n*-octane show two negative CD bands at 319 and 333 nm due to short-axis polarized ^1L_b absorptions. In the gel made slowly by incubation at 40.0 °C, the two bands are red-shifted by 2 and 4 nm, respectively. Another band, at 303 nm, is not prominent when gels are formed rapidly by incubation at 5.4 °C.[6a] Although the origin of this band is unknown at present, we believe that it is due to excitonic interactions that can accompany aggregation of molecules such as **CNC** that contain aromatic moieties.[30]

The final appearance of the CD spectra of the gels is very dependent upon the temperature at which their sols were incubated (Figure 3 and Supporting Information Figure 4), while their UV−vis spectra are not (Supporting Information Figure 3). In the plain-positive regions of the CD spectra, above ∼340 nm, intensity is lower when gels are formed from low-temperature incubations and the signals become negative when higher temperatures are employed. The weak peaks below 340 nm in gels formed at lower temperatures become more intense, but negative in sign, as incubation temperature is increased. The same critical temperature region is observed for those CD changes and the transformations from spherulitic to nonspheru-litic growth patterns noted in optical micrographs.

The inset in Figure 4 is a compilation of time-dependent CD spectra from a 1.0 wt % **CNC**/*n*-octane sample collected at different times after its sol was incubated at 40 °C. The intensity of each band is related to the degree of **CNC** aggregation and, thereby indirectly, to the amount of the gel network present at various times. Only the most intense bands, at ca. 303 and 336 nm, have been used to collect kinetic data. Assuming that no aggregates of **CNC** that are large enough to induce macro-chirality are present at time = 0 (as defined above) and that the aggregation and extent of fibrillar network formation are at their equilibrium values when the CD intensities no longer increase perceptibly with time (i.e., at time = ∞), the fraction of the gel phase at time = t, $X(t)$, can be expressed in terms of the intensities at time = 0, t, and ∞ ($I(0)$, $I(t)$, and $I(∞)$, respectively): $X(t) = (I(t) - I(0))/(I(∞) - I(0))$. Then, values

(30) Kasha, M. *Rev. Mod. Phys.* **1959**, *31*, 162−169.
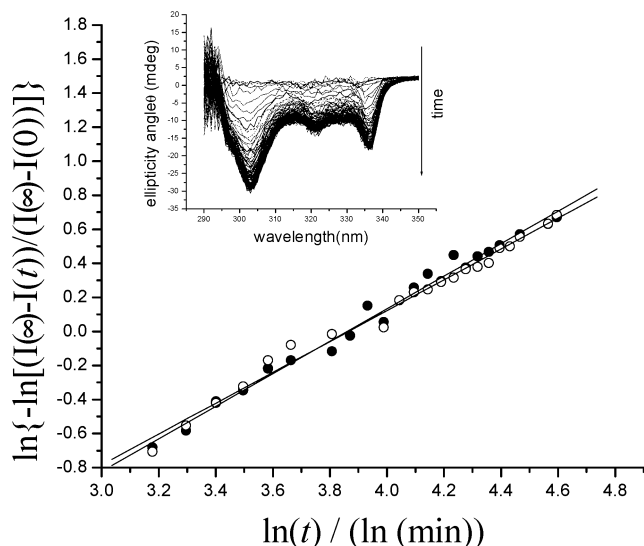
Figure 4. CD spectral intensities at 303 (○; slope = 0.96, R^2 = 0.99) and 336 nm (●; slope = 0.91, R^2 = 0.99) from the inset spectra plotted according to eq 2. Best linear fits of the data are shown. Inset: 1.0 wt % **CNC**/*n*-octane sample incubated at 40 °C; the time period covered is from 0 to 277 min. Each spectrum required 3 min to record.

of K are obtained most easily from single-exponential decay fits of the data using eq 1 (Supporting Information Figure 5), and the Avrami exponent n is most easily extracted from eq 2 by plotting $\ln[-\ln(I(\infty) - I(t))/(I(\infty) - I(0))]$ versus $\ln t$ (Figure 4).

$I(0)$ and $I(\infty)$ must be determined accurately in order to extract meaningful values of n and K.[7b] In the CD experiments, $I(\infty)$ is defined as the average of the band intensities of 20 scans after no perceptible change can be discerned at long times. Due to the stochastic nature of the initial nucleation, an irreproducible induction period of 3−9 min, that increases *qualitatively* as the reduced temperature and the degree of supersaturation decrease, is observed before intensities begin to rise. Zero-time is defined when $I(0)$ begins to increase rapidly; as such, the exact $t = 0$ is somewhat subjective and has more error potentially than $t = \infty$. The uncertainty in both values probably contributes to the slight curvature in plots of the kinetic data. To minimize these errors and to observe the influence of the uncertainty, values of n and K from data treatments in which "zero-time" was advanced or retarded by 3 min were compared; the deviations from the reported values are small.

The Avrami exponents from the slopes in Figure 4 using eq 2, ∼1, imply either a one-dimensional and interface-controlled growth pattern or a two-dimensional and diffusion-controlled growth pattern.[29] Because all of the POM micrographs of the **CNC** gels show fibrillar networks (note that the spherulites are composed of fibers as well), the Avrami exponent here is more compatible with gelation by a one-dimensional and interface-controlled process. Interfacial-controlled growth is a very reasonable mechanism at the concentrations of **CNC** employed, ca. 1 wt % or 1.3×10^{-2} mol/L. In addition, the small n value also indicates an instantaneous (zero-order) nucleation mechanism.[29,31]

The slopes in Figure 4 may also be interpreted as the fractal dimension D_f.[5b,c] Within the fractal model, a value of D_f near 1 also indicates a one-dimensional growth pattern with little

branching.[32] The same conclusion is reached from analyses of the data sets from the fluorescence, SANS, and rheological measurements (vide infra).

An excellent fit to a single-exponential function is obtained when the data are plotted according to eq 1 and using the closest integral n value, 1.0, indicated by the treatment with eq 2 and Figure 4 (Supporting Information Figure 5).

The increase of intensity $I(t)$ between 343 and 347 nm was used to follow aggregation when gels were incubated below 30 °C because the precise peak maximum was difficult to determine (Supporting Information Figure 6, for example). From data treatments according to the Avrami equations (Supporting Information Figures 7 and 8), values of n near 1 were again obtained (Supporting Information Table 2). The relationship between K and temperature will be discussed later.

(c) Degree of Aggregation from Small-Angle Neutron Scattering (SANS). The neutron scattering signal is inconsequential in the sol phase of **CNC** in *n*-dodecane-d_{26}. As gelation proceeds, scattering intensity in specific Q-ranges increases due to increases in the size and number of scattering objects.[3,5a,33] Although a great deal of information concerning the sizes, shapes, and distributions of aggregate objects within an organogel sample can be gleaned from careful analyses of scattering intensity as a function of Q, our interest here is in the *total intensity of scatter over a specific range of Q as a function of time*. Such measurements provide information about the temporal increases of all scattering objects, regardless of their size and shape. As long as the distribution of such objects changes in a regular fashion with time during the gelation process, the integrated intensity of scatter can be treated like the increase in CD signals to obtain meaningful kinetic information about gelation.

The changes in the integrated Q range between 0.008 and 0.1 Å^{-1} for one run with 1.0 wt % **CNC**/*n*-dodecane-d_{26} at 40.0 °C is shown in the inset of Figure 5. The rate of gelation of a higher concentration sample containing 3.0 wt % **CNC** was too fast to be monitored precisely at 40.0 °C by the SANS method (see Supporting Information Figure 9). Here, $I(\infty)$ is defined again as the average of the scattering intensities of the last 20 points recorded after changes in contiguous $I(t)$ measurements became very small. As before, an irreproducible 4−6 min induction period was observed after the 1.0 wt % samples were cooled from the sol phases to a temperature below T_g and prior to a marked increase in scattering intensity. To increase precision, $I(0)$ is defined as the average of the scattering intensities throughout the induction period. The deviations of data points from the best fit lines at very early and very late times are expected from Avrami theory[7,29b] and from the very small differences between $I(\infty)$ and $I(t)$ at late times. As with the CD data, the values of n obtained are always near 1 (Figure 5).

(d) Viscoelastic Changes from Rheological Measurements.[34] Enormous changes of the mechanical properties attend

(31) Tadmor, R.; Khalfin, R. L.; Cohen, Y. *Langmuir* **2002**, *18*, 7146−7150.

(32) Deway, T. G. *Fractals in Molecular Biophysics*; Oxford University Press: New York, 1997.
(33) Guinier, A.; Fournet, F. *Small Angle Scattering of X-rays*; Wiley: New York, 1995.
(34) During some rheological measurements, the values recorded for G′ or other parameters suddenly changed, causing anomalies in the data set. Possible reasons include spikes in the electrical line voltage supply, slippage between a plate surface and a gel (Wilder, E. A.; Hall, C. K.; Khan, S. A.; Spontak, R. J. *Langmuir* **2003**, *19*, 6004−6013), or the movement of small bubbles in contact with a plate..

Figure 5. Avrami plot of data in the inset according eq 2: slope = 1.15 (R^2 = 1.00); the point at earliest time and the three points at the latest times were not included in the linear data fit (see text). Inset: Plot of integrated scattering intensities ($I(t)$) from SANS measurements versus time for a 1.0 wt % **CNC**/*n*-dodecane-d_{26} sample incubated at 40.0 °C.

formation of an organogel, a solidlike material, from a sol or solution, a free-flowing liquid. Thus, kinetic information can be obtained, as well, by following changes in mechanical properties such as the elastic modulus (G'), loss modulus (G''), complex viscosity (η^*), torque, or even stress. Here, we utilize primarily temporal changes in G' (and, in some cases, G'') to follow the kinetics of gelation; there is a clear relationship between the extent of gelator network and G'.[35]

All rheological experiments were performed in *n*-dodecane, rather than *n*-octane, to minimize evaporation from samples at superambient temperatures, and at a low strain (≤1%) well within the linear viscoelastic (LVE) regime.[36] Typical dynamic rheological behavior of a 1.0 wt % **CNC**/*n*-dodecane gel (after equilibration) is shown in Supporting Information Figure 10. It is consistent with the sample being a true gel:[19a] G' is always greater than G'', and both are independent of frequency in the LVE regime.[37] In addition, the complex viscosity η^* decays with a slope −1 in the double logarithmic plot, which, according to eq 3, indicates an infinite viscosity as the shear rate approaches zero and a system with a limited linear viscoelastic domain and a limited yield stress.[38] Analogous behavior of G', G'', and η^* occurs when 1.0 wt % samples are incubated at temperatures ranging from 0 to 40 °C.

$$|\eta^*(\omega)| = (G'^{\,2} + G''^{\,2})^{1/2}/\omega \qquad (3)$$

Although the mechanical perturbations associated with rheological measurements may influence the kinetics of gelation (and inappropriate experimental parameters, such as strain and frequency, may break junctions between fibrils and, thereby,

destroy the gel) or accelerate gelation (rheopexy, leading to higher values of the Avrami *K* parameter),[39] there is no reason to believe that the aggregation patterns, as represented by the values of the Avrami exponent, will be altered. To minimize such effects, all kinetic rheology experiments were performed at 1% strain (well within the LVE) and at 10 rad/s unless stated otherwise. Despite this, the method of placement of the samples between the rheometer plates made the reproducibility of the absolute values of G' and G'' between runs on the same sample or equivalent samples very poor. However, the values of tan δ, the ratios between G'' and G', are reproducible, as they should be if the same type of gel network is formed in each run. At the gel point, tan δ is expected to become independent of frequency.[40]

Because rheometric measurements can be obtained and repeated much more rapidly than those using CD, fluorescence, or SANS, kinetic experiments could be performed at temperatures as low as 0 °C, and they were conducted at 5 °C intervals to 40 °C. In the 0−15 °C range, where no obvious induction time was observed due to the fast nucleation, $G'(0)$ (or $G''(0)$) is defined as the value of G' (or G'') at the time of the first measurement. An induction period was observed at 35.0 and 40.0 °C, allowing $G'(0)$ (or $G''(0)$) to be the average of the G' (or G'') values throughout the induction period. $G'(\infty)$ and $G''(\infty)$ are, again, the average values of the last 20 G' and G'' determinations in each experiment. Here, X(t) in eqs 1 and 2 can be expressed as $[G'(t) - G'(0)]/[G'(\infty) - G'(0)]$ (or a corresponding expression for G'').

At very early times, G' and G'' are very small, indicating a low viscosity liquid (Supporting Information Figure 11). Thereafter, both G' and G'' increase, and the plateau value of G' is much larger than that of G''. Formation of a three-dimensional network is indicated at this point.[37] Qualitatively, the rate of gelation increases with decreasing temperature. Quantitative analyses based on eq 2 yield Avrami exponents ~1, and single-exponential decay fits based on eq 1 provide consistent results (Supporting Information Table 2 and Supporting Information Figures 12 and 13). Analogous treatment of the G'' data gives, again, values of *n* that are very near 1.

The rheological kinetic data from a 1.0 wt % **CNC**/*n*-dodecane sample gelated at 40.0 °C (Figure 6) and 35.0 °C (Supporting Information Figure 14) show an induction period like that seen by the other techniques and, again, it was absent in the lower temperature runs. In addition, two different induction times, t_1 and t_2, are indicated by G' and G'' at 40.0 °C. Closer examination of the G' curve reveals that its patterns of increase during the t_1-t_2 period and after it are different; the nucleation processes within these time regimes must differ in subtle ways. A reasonable hypothesis is that elementary nucleation steps, leading to individual fibrils, occur within the t_1-t_2 period. The fibrils begin to join to form a network thereafter.

We conclude that within the 'instantaneous' nucleation time regime, all nucleation sites are generated very early in the gelation process, but over a finite period (and at a constant rate; see the inset in Figure 6) that is defined by t_1-t_2. During this period, G'' represents the properties of a liquid and remains virtually unchanged. G' is sensitive to the appearance of the

(35) Goodwin, J. W.; Hughes, R. W. *Rheology for Chemists: an Introduction*; The Royal Society of Chemistry: Cambridge, 2000; pp 49, 116.
(36) Khan, S. A.; Royer J. R.; Raghavan, S. R. *Aviation Fuels with Improved Fire Safety: A Proceeding*; National Academy Press: Washington, DC, 1997; pp 31−46.
(37) Lortie, F.; Boileau, S.; Bouteiller, L.; Chassenieux, C.; Demé, B.; Ducouret, G.; Jalabert, M.; Lauprêtre, F.; Terech, P. *Langmuir* **2002**, *18*, 7218−7222.
(38) (a) Terech, P.; Pasquier, D.; Bordas, V.; Rosat, C. *Langmuir* **2000**, *16*, 4485−4494. (b) Doraiswamy, D.; Mujumdar, A. M.; Tsao, I.; Beri, A. N.; Danforth, S. C.; Metzner, A. B. *J. Rheol.* **1991**, *35*, 647−685. (c) Ferry, J. D. *Viscoelastic properties of polymers*; John Wiley: New York, 1980.

(39) Steg, I.; Katz, D. *J. Appl. Polym. Sci.* **1965**, *9*, 3177−3193.
(40) Winter, H. H.; Chambon, F. *J. Rheol.* **1986**, *30*, 367−382.
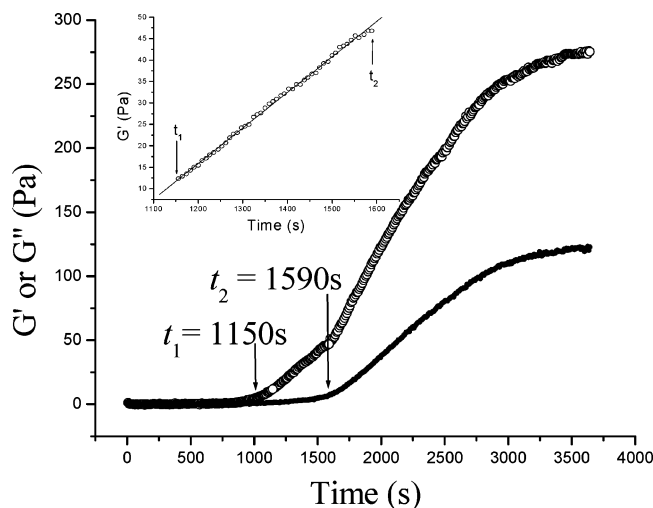
Figure 6. Dynamic rheological data for a 1.0 wt % **CNC**/*n*-dodecane sample undergoing gelation at 40.0 °C. The main figure shows the evolution of the elastic modulus G' (○) and the viscous modulus G'' (●) recorded at a frequency of 10 rad/s and a strain of 1%. Inset: G' versus time during the t_1-t_2 period; the best linear fit to these data has a slope = 0.08 Pa/s ($R^2 = 1.00$).

Figure 7. Avrami plot of fluorescence data in the inset according eq 2 (slope = 1.08 ($R^2 = 1.00$)). Inset: Plot of emission intensity (λ_{em} 375 nm; λ_{ex} 318 nm) from a 1.0 wt % **CNC**/*n*-octane sample incubated at 1.1 °C.

second phase (fibrils) and changes significantly during the t_1-t_2 period. Although the quantitative aspects of these changes are not reproducible (for reasons mentioned earlier), the qualitative aspects of the development of the gel structure are found in every run at the higher incubation temperatures.

Multiple waveform rheology is a technique that applies a compound waveform on the sample to determine the gel point in a single experiment (see Supporting Information).[41] No clear gel point (defined by time at constant temperature in our experiments) was discernible when this technique was applied to 1.0 wt % **CNC**/*n*-dodecane samples at 35.0 and 40.0 °C (Supporting Information Figures 15 and 16). However, interesting kinetic information was obtained. The Avrami exponents from these experiments are again near one, as are those from analogous plots using G'' values (Supporting Information Table 2). At both temperatures, the G' and G'' values increase according to a single-exponential function; the presence of a linear-increase region like that found in the time-sweep experiments at the same temperatures is less clear, and none was obvious in plots of CD, SANS, or fluorescence derived data at 35 and 40 °C. In addition, initial linear-growth regions were absent in rheological experiments conducted at lower temperatures. If present, they would have escaped our detection due to the very rapid nucleation.

To explain the linear increase regions and their detection only by rheological measurements, we suggest that aggregates not incorporated within a gelator network (individual fibrils) dominate during the t_1-t_2 regime while those within the network are prevalent after t_2. If this hypothesis is correct, the absence of a detected linear region in the CD, SANS and fluorescence (vide infra) experiments can be attributed to the inability of these techniques to differentiate between the two types of fibrils. Nonlinear increases of the moduli begin when the population of incipient fibrils becomes sufficiently large to allow cross-links and the SAFIN to develop. Clearly, additional experiments will be required to test this hypothesis.[42]
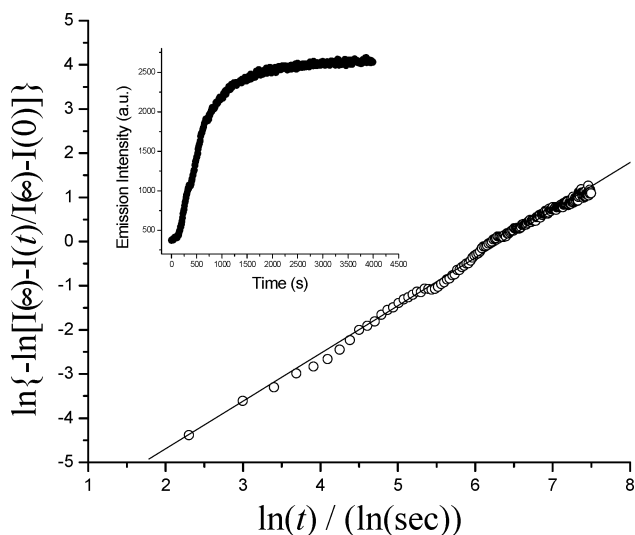
(e) Kinetics of Aggregation by Fluorescence. Naphthyl groups of **CNC** molecules fluoresces strongly after being excited to their S_1 state. The emission maximum of the *n*-alkane gels (357 nm) is red-shifted by about 7 nm from that of the sols due to the intermolecular associations and interactions mentioned in discussion of the CD data. The time periods necessary for introduction of the sol samples into the thermostated fluorometer sample holder and for obtaining each datum are shorter than the times associated with the same operations using the CD, SANS, and rheological techniques. As a result, precise time = 0 data (i.e., before the end of the induction periods) can be obtained even during lower temperature experiments. To maximize reproducibility and minimize uncontrollable variables (such as the concentration of dust particles or nucleation sites on the glass surfaces), the same sample for each concentration of **CNC** was employed in fluorescence runs at different temperatures. Thus, kinetic fluorescence data yielded reproducible values for K and consistent trends for its temperature dependence.

A typical kinetic plot from a fluorescence experiment at the lowest temperature investigated (and, therefore, the most difficult to determine the intensity at time = 0) is shown in Figure 7. The dependence of the kinetics of gelation on **CNC** concentration was also examined by fluorescence. Within the concentration (0.89−3.0 wt %) and temperature[5a,7] ranges (1.1−39.2 °C) explored, the values of the Avrami exponent n remained again near one (Supporting Information Tables 2 and 3).

(f) Relationship between K, Temperature, and Concentration. According to the data from the four methods for following the kinetics of gelation of **CNC** in the two *n*-alkanes, the Avrami exponent n remains near one, even when the LMOG concentration and temperature are changed (Supporting Information Tables 2 and 3).[5a,7] As noted above, K is predicted to be temperature and concentration dependent, and it does vary with both, but in a completely unexpected way.

(41) Raghavan, S. R.; Chen, L. A.; McDowell, C.; Khan, S. A. *Polymer* **1996**, *37*, 5869−5875.

(42) An analogous linear increase followed by a nonlinear increase of G' has also been observed during formation of a peptide hydrogel: Lamm, M. S.; Rajapopal, K.; Schneider, J. P.; Pochan, D. J. *Abstracts of Papers,* 17th Polymer Network Group Meeting, Bethesda, MD, August 15−19, 2004.
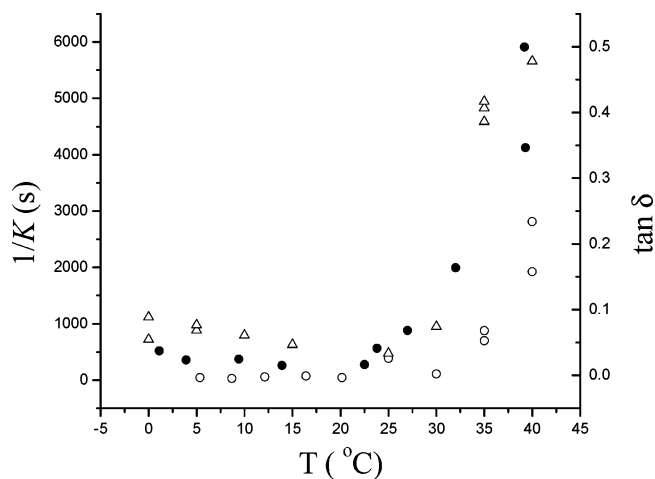
Figure 8. $1/K$ values (from fluorescence (●) and CD (○) data based on eq 1) and tan δ (△, from rheology measurements at 10 rad/s) versus temperature. In all cases, **CNC** was 1.0 wt %; the liquid was *n*-octane for the spectroscopic samples and *n*-dodecane for the rheology ones.

Figure 8 is a plot of the temperature dependence of $1/K$ (or "time constant" for gelation) values obtained from eq 1 using fluorescence and CD spectroscopic data as well as limiting tan δ values (the ratio of G''/G' within the plateau regions) from rheological experiments. The three data sets are remarkably internally and externally consistent, and the common trend is clear: there is one region of very small and another of very large temperature dependence. Quantitative differences arise because the conditions under which the experiments are very difficult to reproduce exactly and each of the techniques measures a somewhat different aspect of the aggregation/gelation process.

The broad temperature range for the change from low to high dependence of $1/K$ on temperature indicates a gradual "transition". No evidence for a first-order phase transition in this temperature regime is found in differential scanning calorimetry thermograms of neat **CNC** or in X-ray diffractograms of the **CNC** gels. However, *the gradual change detected in the optical micrographs from spherulitic to nonspherulitic growth in the gels does occur in the vicinity of the temperature excursions in Figure 8.*

The relationship between K and **CNC** concentration is more complicated. As shown in Figure 9, $1/K$ is independent of concentration at low incubation temperatures but increases with decreasing concentrations at higher temperatures. Based upon the appearances of the corresponding optical micrographs, the changes at higher temperatures are due to the transformation from spherulitic to long fiber growth patterns.

An Arrhenius-type plot of the $1/K$ and tan δ values using the reduced temperature, $T_g - T$, and an average value of the T_g in Table 1 from different cooling protocols (52 °C) does not yield good linear fits (Figure 10) due, in part, to the uncertainty in T_g. Despite the scatter in the data, their approximate slopes suggest "activation energies", ∼95−135 cal/mol, that are much smaller than even those for self-diffusion of the liquid components, *n*-octane (2.6 kcal/mol) and *n*-dodecane (3.2 kcal/mol)-![43] Insofar as this treatment is meaningful, it suggests that the "rate-limiting" step in the aggregation process involves very

(43) von Meerwall, E.; Beckman, S.; Jang, J.; Mattice, W. L. *J. Chem. Phys.* **1998**, *108*, 4299−4304.
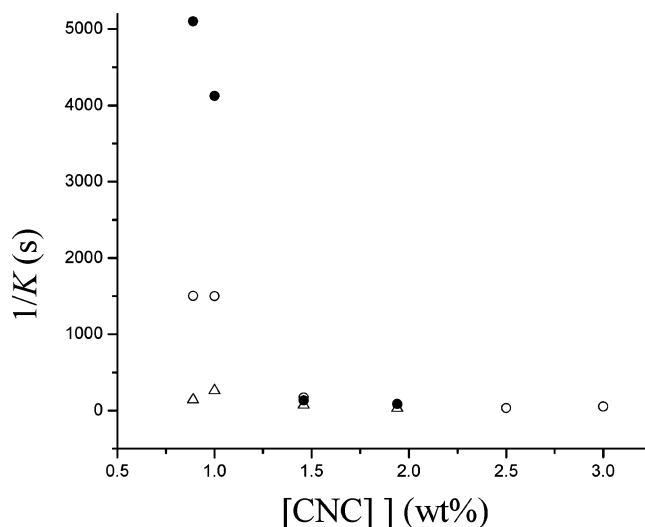
Figure 9. $1/K$ values from fluorescence data (λ_{ex} 318 nm, λ_{em} 375 nm) versus **CNC** concentration in *n*-octane at 36.3 (●), 32.2 (○), and 14.5 °C (△).
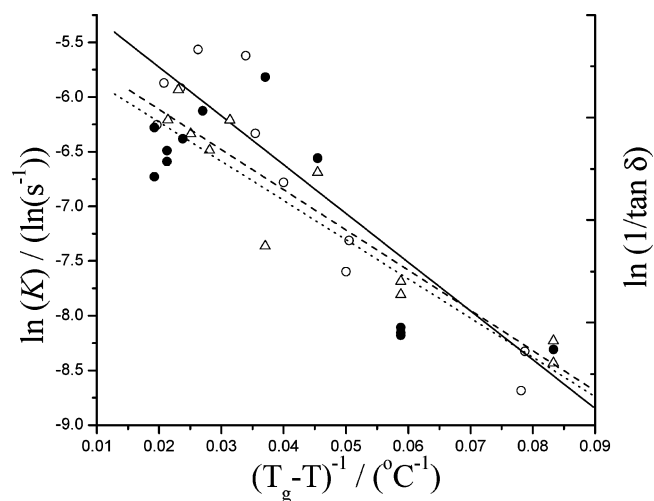

Figure 10. Arrhenius-type plots of K (from fluorescence (○, $R^2 = 0.94$) and CD (△, $R^2 = 0.95$; data based on eq 1), and tan δ (●, $R^2 = 0.82$, from rheology measurements at 10 rad/s) using reduced temperature. In all cases, **CNC** was 1.0 wt %; the liquid was *n*-octane for the spectroscopic samples and *n*-dodecane for the rheology samples.

little motion of **CNC** molecules in sols, perhaps a subtle expulsion of liquid molecules. As such, it is not typical of bulk crystal growth, at least after the initial nucleation stages.[4]

Conclusions

Fluorescence and circular dichroic spectroscopic measurements, small angle neutron scattering data, and rheological changes have been used to follow the kinetics of gelation of two *n*-alkanes by 5α-cholestan-3β-yl *N*-(2-naphthyl)carbamate. The results have been analyzed primarily using an Avrami model. The four techniques begin their investigation of the gelation process at different length scales and steps in the aggregation/self-assembly process, and yet all lead to the same conclusion: gelation occurs via instantaneous nucleation and one-dimensional growth.[31,44] This conclusion is supported by the fibrous networks that are seen in optical micrographs of the fully formed gels.

(44) (a) Jackson, C. L.; Shaw, M. T. *Polymer* **1990**, *31*, 1070−1084. (b) Horton, J. C.; Donald, A. M. *Polymer* **1991**, *32*, 2418−2427.

The rheological measurements have revealed different influences of the growth of small (early stage) and larger (late stage) aggregates on viscosity, a phenomenon that was not detected by any of the other techniques. SANS measurements demonstrate that relatively large aggregates continue Avrami-type growth until gelation is complete. Fluorescence measurements probe the earliest steps in the aggregation phenomenon, when liquid molecules are excluded from the space between groups of vicinal **CNC** molecules, and then growth after nucleation. Finally, the CD technique probes the nature of the molecular packing within aggregates of sizes sufficient to express macrohelicity.

In toto, the results provide a comprehensive picture of exceedingly complex self-assembly processes and allow us to decipher specific changes in the kinetics that result in spherulitic (colloidal) or rodlike (long fibrillar) objects within the gel networks. There is an unusual link[6a] between the temperature and, therefore, kinetics of gelation by **CNC** and the morphology of its gel networks. The temperature range associated with the morphological transition corresponds to drastic changes in the Avrami K "rate constants" obtained by SANS, fluorescence, and rheological measurements. The self-consistency of the Avrami parameters from the four interrogation techniques gives us confidence that our conclusions concerning the one-dimensional growth modes and the link between the morphological changes of the SAFINs and the kinetics of their formation are correct.

The body of data indicate that initial nucleation—which is largely dependent on the nature of the gelator,[5,31] the degree of supersaturation (i.e., $T_g - T$), and heterogeneities (supersaturation or the presence of particles such as dust) within the system[24]—determines the morph of the final gel when its solution or sol is cooled below T_g. In that regard, the earliest stages of aggregation and self-assembly are nebulously characterized,[24] but extremely important, period in the gelation process.[45] It is difficult to define the period when they begin and to separate them from subsequent growth of LMOG objects. Regardless, this study has provided valuable insights into that period and, especially, later ones. It demonstrates the delicate relationship among several competing kinetic factors that lead to different forms of a SAFIN gel[46] (or, perhaps, physiologically relevant fibrillar assemblies,[10−18] and provides an empirical approach to characterizing their temporal and structural aggregation steps, including those at the early stages of self-assembly.

Supporting Information Available: Experimental details and additional spectroscopic and kinetic data, including tables of Avrami parameters, for **CNC**/*n*-alkane gels at several concentrations and temperatures. This material is available free of charge via the Internet at http://pubs.acs.org.

JA0426544

(45) George, M.; Weiss, R. G. *Langmuir* **2003**, *19*, 8168−8176.
(46) (a) Spector, M. S.; Selinger, J. V.; Schnur, J. M. In *Materials Chirality*; Green, M. M., Nolte, R. J. M., Meijer, E. W., Eds.; John Wiley and Sons: New York, 2003, Chapter 5. (b) Aggeli, A.; Nyrkova, I. A.; Bell, M.; Harding, R.; Carrick, L.; McLeish, T. C. B.; Semenov, A. N.; Boden, N. *Proc. Natl. Acad. Sci. U.S.A.* **2001**, *98*, 11857−11862.

Kinetics of 5α-cholestan-3β-yl N-(2-naphthyl) carbamate/*n*-alkane organogel formation and its influence on the fibrillar networks

Xiao Huang,[1] Pierre Terech,[2] Srinivasa R. Raghavan,[3]and Richard G. Weiss[1]*

[1]*Department of Chemistry, Georgetown University, 37th and O Streets, NW, Washington, DC 20057-1227 USA,* email: weissr@georgetown.edu
[2]*CEA-Grenoble, DRFMC/SI3M Laboratoire Physico-Chimie Moleculaire 17, Rue des Martyrs 28054 Grenoble cedex 9, France*
[3]*Department of Chemical Engineering, University of Maryland, College Park, MD 20742-2111 USA*

Experimental Section

Materials. *n*-Octane (Aldrich, 98%), *n*-dodecane (Acros, 99+%), and *n*-dodecane-d_{26} (MSD Isotopes, 98 atom% D) were used as received. 5α-Cholestan-3β-yl N-(2-naphthyl) carbamate (**CNC**) was synthesized as described in the literature[1] to yield material of mp 184.1-184.9 °C (lit mp 178 - 180 °C[1]). Elemental Analysis: calcd for $C_{38}H_{55}NO_2$, C 81.82%, H 9.94%, N 2.51%; found, C 81.83%, H 10.38%, N 2.53%. ^{1}H-NMR: 8.00, 7.80-7.72, 7.46-7.28 (m, 7H, aromatic), 6.72 (s, 1H, NH), 4.80-4.65 (m, 1H, CH), 2.20-0.60 ppm (m, 47H, cholestanyl).

Instrumentation and sample preparation. Samples for gelation studies were prepared by placing known amounts of solvent and **CNC** in 5 mm (i.d.) glass tubes or 0.5 or 0.8 mm pathlength flattened capillaries. The containers with the gel components were flame-sealed and then heated until the gelator completely dissolved. Thereafter, the hot solutions/sols were cooled by different protocols until gelation occurred. They included

submerging the tubes in an ice-water bath (fast cooling), placing the tubes in air at ambient temperature (moderate cooling), or submerging the tubes in a thermostatted bath set at a temperature below T_g (controlled cooling). Qualitatively, gelation was considered successful if no sample flow was observed upon inverting the container at room temperature (i.e., the 'inverse flow' method[2]) after a third heating and cooling cycle. If part of the sample fell, the sample was classified as a partial gel.   More detailed determinations of gel formation were provided by rheology measurements (vide infra).

Optical micrographs were recorded on a Leitz 585 SM-LUX-POL microscope equipped with crossed polars, a Leitz 350 heating stage, a Photometrics CCD camera interfaced to a computer, and an Omega HH503 microprocessor thermometer connected to a J-K-T thermocouple. The samples, sealed in 0.5mm thickness flatted capillary tubes, were heated to their isotropic phase in a boiling water bath and cooled in an ethylene glycol bath that was equilibrated at a designated temperature.   Optical micrographs were recorded after the samples were in the bath for 30 minutes (incubation at < 30 °C) or overnight (incubation at > 30 °C) to ensure that gelation had occurred.

UV spectra were obtained using a Cary 300 BIO UV-vis spectrophotometer. Fluorescence spectra were recorded on Spex Fluorolog III spectrometer equipped with a VWR-1140 circulating thermostatting bath.

X-ray diffraction (XRD) of samples was performed on a Rigaku R-AXIS image plate system with Cu Kα X-rays (λ = 1.54056 Å) generated by a Rigaku generator operating at 46 kV and 46 mA with the collimator at 0.3 mm. Data processing and analyses were

performed using Materials Data JADE (version 5.0.35) XRD pattern processing software. Samples were sealed in either 1.0 mm (gels, exposures for 10 h) or 0.5 mm (neat powder, exposure for 30 min) glass capillaries (W. Müller, Schönwalde, Germany).

   Kinetics of gelation by CD spectroscopy. **CNC**, dissolved in hot *n*-octane, was transferred to a 1.0 mm thick water-jacketed CD cell that was kept at 90 ºC. CD spectra were recorded on a Jasco-700 CD spectrometer immediately after liquid at a predetermined temperature was flowed from a thermostatting circulating bath through the jacket of the cell.   'Zero' time was defined as when the first spectrum was recorded; the approximate period required for temperature equilibration after sample transfer was less than 30 seconds since a very small amount of sample was used. The shortest period to complete gelation was 10-15 min. The scan rate and other instrumental parameters were set to optimize the signal-to-noise ratio. Infinite time values, when spectra no longer changed perceptibly with time (i. e., gelation was complete), were the average of signals from twenty scans.

   Kinetics of gelation by fluorescence spectroscopy. **CNC** and *n*-octane in a sealed 3 mm pathlength flattened quartz tube or a 0.8 mm pathlength flattened Pyrex tube was heated until all solids dissolved. Then, the tube was placed into a thermostatted cell holder of the fluorimeter and the emission intensity at 375 nm (excitation at 318 nm) was recorded from the front-face as a function of time at a rate of 1 datum per second. In the data treatment, sets of 10 or 100 consecutive points were averaged and fitted to the kinetic models.

Kinetics of gelation by small angle neutron scattering (SANS). Data were obtained on

the 30 m SANS beam line at the National Center for Neutron Research of the National

Institute of Standards and Technology, Gaithersburg, MD (5 m scattering, $\lambda = 8.09$ Å)

using 2 mm pathlength cylindrical quartz cells placed in a thermostatted ($\pm$ 0.1 ºC) cell

holder.   Hot samples (with *n*-dodecane-d_{26} as the liquid) were transferred to the

thermostatted cells as described above.   The delay between the moment of transfer and

initial measurements was less than 10 s.   In the kinetic runs, intensity data were summed

over a *Q* range of 0.008-0.1 Å^{-1} for 10 s increments with 35 s delays between collections.

Kinetics of gelation by rheological measurements. Rheology data were recorded on a

Rheometric Scientific RDA III rheometer equipped with parallel plates (25 mm diameter)

and Peltier-based temperature control ($\pm$0.1 °C) samples. The gap between the plates

(0.3-0.5 mm) did not influence mechanical properties of the samples, as indicated by the

elastic modulus (G'), the loss modulus (G''), the ratio between G'' and G' (tanδ), and the

complex viscosity (η*). Dynamic rheological experiments were performed between 0.01

and 100 rad/s at a constant strain (1%) that was well within the linear regime of

deformation. Hot solutions of **CNC** in *n*-dodecane were transferred onto the lower plate

that was at 40 °C when the desired temperature was higher than 20 °C or at 20 °C higher

than the desired temperature when the desired temperature was below 20 °C. The plate

was cooled quickly (ca. 30 s) to the desired temperature after the plate gap was adjusted

to the desired separation. Recording of data commenced immediately thereafter. To

minimize evaporation of the solvent, a solvent trap with a liner soaked with *n*-dodecane was placed over the apparatus when measurements were made at 35 or 40 °C.

Multiple waveform rheology is a technique that applies a compound waveform on the sample, as described in equation 1.[3] γ, the total applied strain, is the sum of the Fourier series described by each individual strain. ω_i, the applied frequencies, are harmonics (integer multiples) of a fundamental frequency. In our experiment, the fundamental frequency was 1 rad/s and the harmonic frequencies were 5, 10, 50, and 100 rad/s. Since the strain for each frequency is 0.2%, their sum γ, 1%, is well within the linear regime of deformation.

$$\gamma = \sum_{i=1}^{m} \gamma_i \sin(\omega_i t) \tag{1}$$

Supporting Table 1. Gelation procedures and appearances of **CNC**/*n*-alkane samples.[a]

[CNC], wt%	Liquid	Gelation protocol[b]	Stability period[c]	Phase notations	T_g (°C)
0.80	*n*-dodecane	Slow	-	Precipitate	-
0.80	*n*-dodecane	Fast	-	Precipitate	-
1.1	*n*-dodecane	Slow	> 5 days	Translucent, strong gel[d]	38.5-58.1
1.1	*n*-dodecane	Moderate	~1-2 days	Translucent, weak gel[d,e]	53.0-53.5
1.1	*n*-dodecane	Fast	< 1 day	Translucent, weak gel[d,e]	42.3-51.5
0.89	*n*-octane	Slow	> 1week	Translucent, strong gel	47.4-49.8
0.89	*n*-octane	Moderate	~ 2 days	Translucent, weak gel	41.0-49.7
0.89	*n*-octane	Fast	-	Partial gel	-
1.0	*n*-octane	Slow	> 6 months	Translucent, strong gel[d]	51.8-56.7
1.0	*n*-octane	Moderate	~1-2 days	Translucent, weak gel[d]	40.5-56.2
1.0	*n*-octane	Fast	<1 day	Translucent, weak gel[d]	52.0-52.2
1.5	*n*-octane	Slow	> 1week	Translucent, strong gel	63.2
1.5	*n*-octane	Moderate	~ 2 days	Translucent, weak gel	62.1-63.5
1.5	*n*-octane	Fast	< 1 day	Translucent, weak gel	62.5-64.2
1.9	*n*-octane	Slow	> 1week	Translucent, strong gel	69.5
1.9	*n*-octane	Moderate	~ 2 days	Translucent, strong gel	69.0-69.5

1.9	n-octane	Fast	< 1 day	Translucent, weak gel	72.1-73.0
3.0	n-octane	Slow	> 1week	Opaque, strong gel	70.2-81.4
3.0	n-octane	Moderate	~ 2 days	Opaque, strong gel	79.5
3.0	n-octane	Fast	< 1 day	Translucent, strong gel	80.1-80.4

[a] A 1 wt% concentration corresponds to ca. 1.3×10^{-2} mol/L. [b] Fast gelation—sol immersed in an ice-water bath; moderate—sol cooled in air; slow—sol cooled in a water bath at 40 °C. [c] Period before macroscopic phase separation at ambient temperature in a sealed container. [d] Weak gel—flow upon mild agitation (shaking by hand); strong gel—no flow induced by mild agitation. [e] Thixotropic; a stronger gel reformed after agitation.

Supporting Table 2. Summary of K and n values from analyses of kinetic experiments on gelation of 1.0 wt% **CNC** in n-alkane samples incubated at different temperatures.

Method	Liquid	Temp (°C)	n [a]	K (s^{-1}) [b]	R^2 [c]
CD	n-Octane	40.0	0.97±0.02 (303nm)	$(5.99\pm0.06) \times 10^{-4}$	0.93
	n-Octane	40.0	1.01±0.02 (337nm)	$(5.19\pm0.09) \times 10^{-4}$	0.95
	n-Octane	40.0	0.91±0.04 (303nm)	$(3.59\pm0.06) \times 10^{-4}$	0.99
	n-Octane	40.0	0.96±0.02 (337nm)	$(3.56\pm0.05) \times 10^{-4}$	0.99
	n-Octane	35.0	1.00±0.02 (302nm)	$(1.11\pm0.04) \times 10^{-3}$	0.98
	n-Octane	35.0	1.28±0.03 (336nm)	$(1.14\pm0.07) \times 10^{-3}$	0.95
	n-Octane	35.0	0.91±0.02 (302nm)	$(1.79\pm0.02) \times 10^{-3}$	0.97
	n-Octane	35.0	1.23±0.05 (336nm)	$(1.44\pm0.09) \times 10^{-3}$	0.95
	n-Octane	30.0	1.18±0.04 (344nm)[d]	$(9.94\pm0.10) \times 10^{-3}$	0.99
	n-Octane	25.0	0.98±0.05 (344nm)[d]	$(2.61\pm0.07) \times 10^{-3}$	0.99
	n-Octane	20.2	1.02±0.02 (344nm)[d]	$(2.25\pm0.06) \times 10^{-2}$	0.99
	n-Octane	1.4	1.22±0.04 (344nm)[d]	$(1.34\pm0.06) \times 10^{-2}$	0.99
	n-Octane	12.1	1.19±0.05 (344nm)[d]	$(1.78\pm0.04) \times 10^{-2}$	0.98
	n-Octane	8.7	0.96±0.02 (344nm)[d]	$(3.45\pm0.07) \times 10^{-2}$	0.99
	n-Octane	5.4	1.06±0.03 (344nm)[d]	$(2.26\pm0.09) \times 10^{-2}$	0.99
SANS	n-Dodecane-d_{26}	40.0	1.09±0.02	$(8.79\pm0.06) \times 10^{-5}$	0.99
	n-Dodecane-d_{26}	40.0	1.15±0.02	$(7.90\pm0.04) \times 10^{-5}$	1.00
Rheology	n-Dodecane	0.0[e]	1.25±0.02	$(9.78\pm0.12) \times 10^{-3}$	1.00
	n-Dodecane	5.0[e]	1.29±0.02	$(1.65\pm0.07) \times 10^{-2}$	0.99
	n-Dodecane	10.0[e]	1.28±0.04	$(4.73\pm0.09) \times 10^{-3}$	1.00
	n-Dodecane	15.0[e]	1.21±0.04	$(9.48\pm0.14) \times 10^{-3}$	0.99
	n-Dodecane	35.0[e]	1.01±0.02	$(4.03\pm0.09) \times 10^{-3}$	0.99
	n-Dodecane	40.0[e]	1.26±0.03	$(8.79\pm0.07) \times 10^{-4}$	1.00
	n-Dodecane	35.0[f]	1.00±0.02 (1 rad/s)	$(4.87\pm0.09) \times 10^{-4}$	1.00
	n-Dodecane	35.0[f]	1.03±0.03 (5 rad/s)	$(4.80\pm0.07) \times 10^{-4}$	1.00

	n-Dodecane	35.0[f]	1.09±0.05 (10 rad/s)	$(4.76\pm0.10) \times 10^{-4}$	1.00
	n-Dodecane	35.0[f]	1.14±0.02 (50 rad/s)	$(4.15\pm0.06) \times 10^{-4}$	1.00
	n-Dodecane	35.0[f]	1.16±0.05 (100 rad/s)	$(3.98\pm0.04) \times 10^{-4}$	1.00
	n-Dodecane	40.0[f]	1.04±0.05 (1 rad/s)	$(9.63\pm0.11) \times 10^{-4}$	0.99
	n-Dodecane	40.0[f]	1.05±0.02 (5 rad/s)	$(1.07\pm0.06) \times 10^{-3}$	1.00
	n-Dodecane	40.0[f]	1.00±0.02 (10 rad/s)	$(1.06\pm0.06) \times 10^{-3}$	1.00
	n-Dodecane	40.0[f]	1.11±0.03 (50 rad/s)	$(9.94\pm0.09) \times 10^{-4}$	1.00
	n-Dodecane	40.0[f]	1.11±0.03 (100 rad/s)	$(9.58\pm0.07) \times 10^{-4}$	1.00
Fluorescence[g]	*n*-Octane	1.1	1.08±0.02	$(1.92\pm0.14) \times 10^{-3}$	1.00
	n-Octane	3.9	1.11±0.02	$(2.82\pm0.09) \times 10^{-3}$	1.00
	n-Octane	9.4	0.97±0.02	$(2.69\pm0.07) \times 10^{-3}$	1.00
	n-Octane	13.9	1.20±0.03	$(3.83\pm0.09) \times 10^{-3}$	1.00
	n-Octane	22.5	1.28±0.02	$(3.62\pm0.06) \times 10^{-3}$	1.00
	n-Octane	23.8	0.98±0.02	$(1.78\pm0.06) \times 10^{-3}$	1.00
	n-Octane	32.0	0.99±0.02	$(5.02\pm0.12) \times 10^{-4}$	0.99
	n-Octane	39.2	1.16±0.02	$(1.69\pm0.07) \times 10^{-4}$	1.00

[a] From linear Avrami fit. [b] From single exponential decay Avrami fit. [c] Square of correlation coefficient based on a linear fit. [d] Average of intensities between 343 and 347 nm. [e] Time-sweep experiments. [f] Multiple wave-form experiments. [g] λ_{ex} 318nm, λ_{em} 375 nm.

Supporting Table 3. Concentration and temperature dependence of Avrami parameters from fluorescence experiments on samples in *n*-octane[a]

Temp (°C)	[CNC] (wt%)	*n*	K (s^{-1})	R^{2} [b]
14.5	0.89	1.19±0.02	$(8.75\pm0.09)\times10^{-3}$	0.98
14.5	1.0	1.18±0.02	$(3.83\pm0.09)\times10^{-3}$	1.00
14.5	1.5	0.97±0.03	$(1.89\pm0.10)\times10^{-2}$	0.99
14.5	1.9	0.98±0.06	$(3.30\pm0.19)\times10^{-2}$	0.99
32.2	0.89	0.98±0.02	$(7.02\pm0.06)\times10^{-4}$	0.99
32.2	1.0	0.99±0.05	$(6.67\pm0.07)\times10^{-4}$	0.99
32.2	1.5	0.96±0.04	$(9.43\pm0.09)\times10^{-3}$	1.00
32.2	1.9	0.98±0.04	$(1.24\pm0.05)\times10^{-2}$	0.99
32.2	2.5	1.12±0.02	$(3.01\pm0.11)\times10^{-2}$	0.99

|				
32.2	3.0	1.07±0.02	(1.93±0.09)×10^{-2}	0.99
36.3	0.89	1.35±0.04	(2.27±0.08)×10^{-4}	0.99
36.3	1.5	1.14±0.02	(9.01±0.12)×10^{-3}	0.99
36.3	1.9	1.00±0.02	(1.20±0.07)×10^{-2}	0.99

[a] λ_{ex} 318nm, λ_{em} 375nm, front-face geometry; [b] Square of correlation coefficient based on a linear fit.
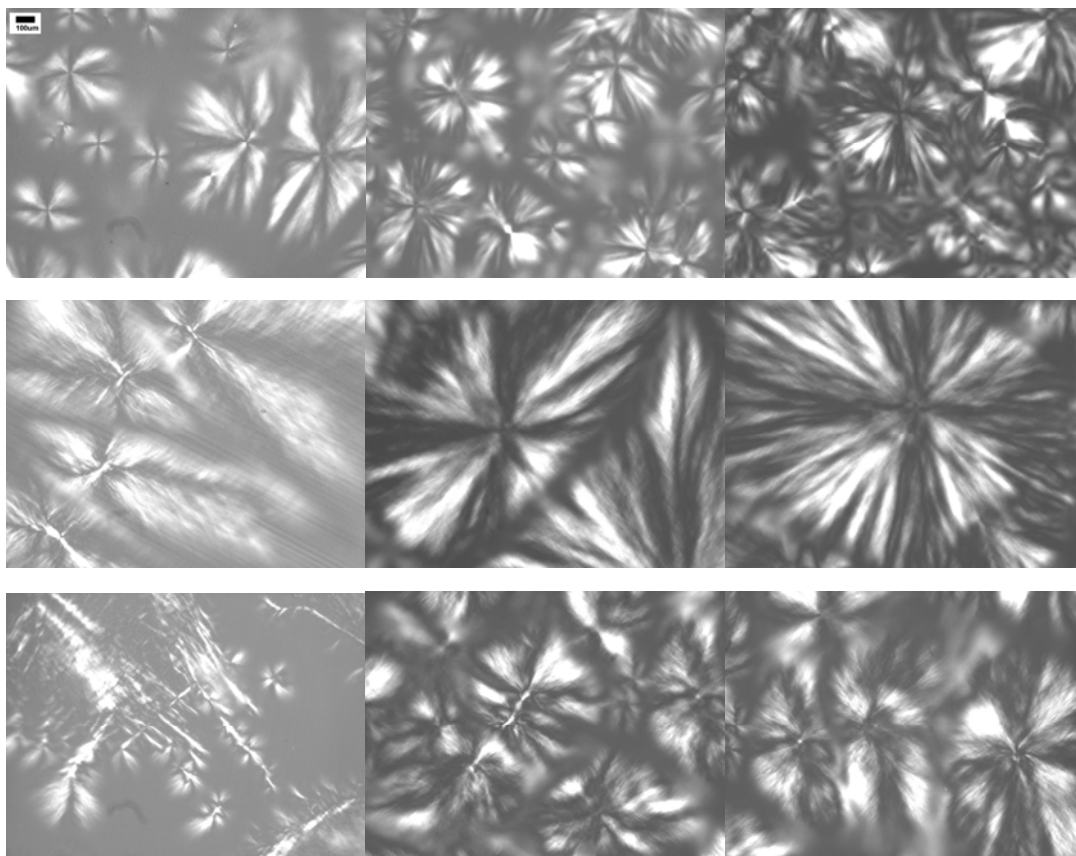
Supporting Figure 1. Optical micrographs of **CNC**/*n*-octane organogels. From left to right: 0.89, 1.46 and 1.94 wt% **CNC**; from top to bottom: incubated at 14.5, 32.2 and 36.3 °C after cooling from well above T_g. The scale bar, 100μm, applies to all micrographs.
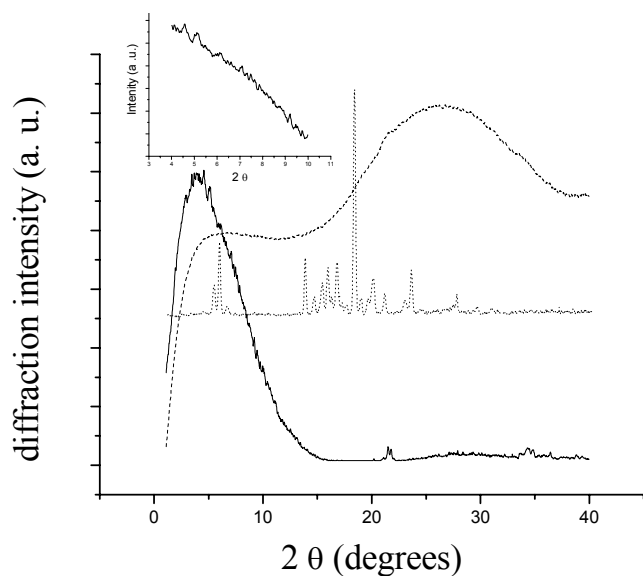
Supporting Figure 2. XRD patterns of a 1.0 wt% **CNC**/*n*-octane gel (incubation at 0 °C after heating above T_g, ----), gel diffraction with an empirical subtraction of the diffraction by neat octane (—), and the diffraction of neat solid **CNC** (····).   The inset is an amplification of peaks from the gel in the low angle region.
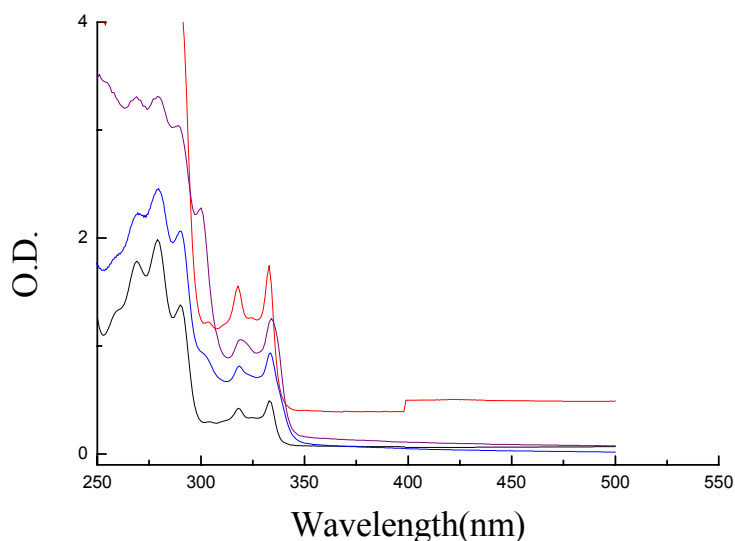
Supporting Figure 3. UV-vis spectra of **CNC**/*n*-octane organogels and solutions: 0.02 wt% solution (red, 5 cm pathlength); 0.19 wt% solution (black, 1 mm pathlength); 1.0 wt% gel formed at 40 °C (purple, 1mm pathlength) and 1.0 wt% gel formed at 0 °C (blue, 1 mm pathlength). Gelated samples were incubated at the temperatures noted after being cooled from well above T_g.
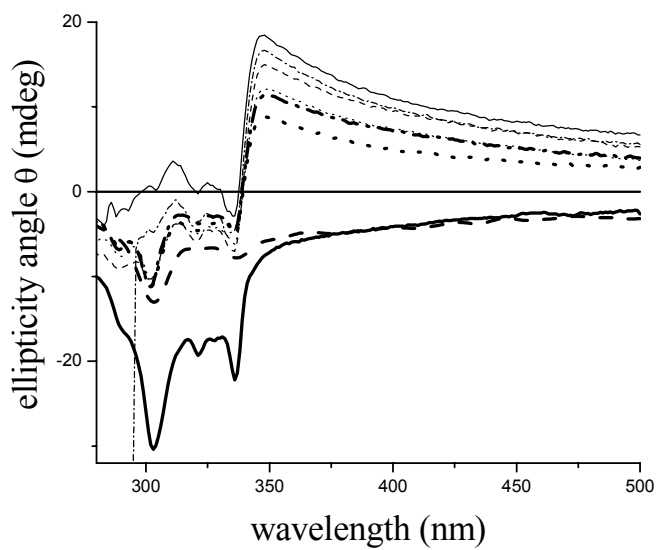
Supporting Figure 4. CD spectra of 1.0 wt% CNC/*n*-octane gels formed upon incubation at 5.4 (—), 8.7 (----), 12.1 (····), 20.2 (-··-), 25.0 (— • —), 30.0 (••••), 35.0 (— —) and 40.0 °C (▬) after being cooled from well above T_g.
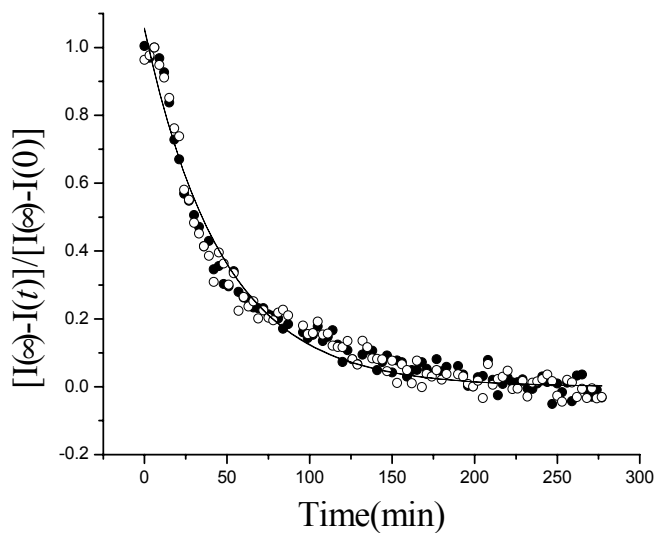
Supporting Figure 5. CD spectral intensities from bands at 303 (●;Y = $1.05e^{(-x/46.48)}$, R^2 = 0.98) and 336 nm (○;Y = $1.05e^{(-x/46.88)}$, R^2 = 0.98) of a 1.0 wt% **CNC**/*n*-octane sample incubated at 40 °C (after being heated above T_g). The two lines representing the best fits to the exponential form of the Avrami equation (see parentheses) are nearly superimposed.
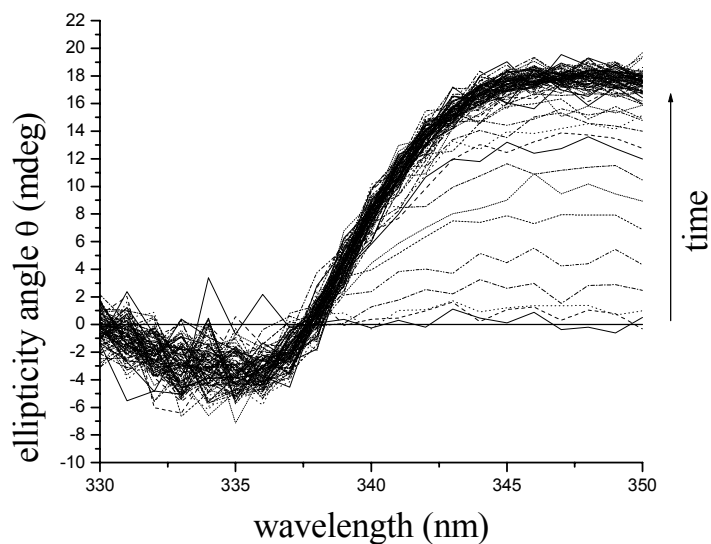
Supporting Figure 6. CD spectra associated with gelation of a 1.0 wt% **CNC**/*n*-octane sample incubated at 5.4 °C after being cooled from well above T_g. The time period covered is from 0 to 814 seconds.
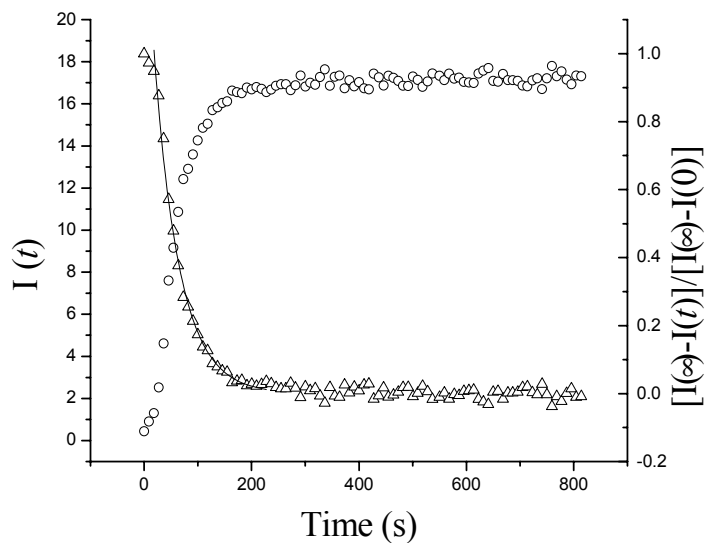
Supporting Figure 7. Plots of I(*t*) from CD experiments (o, average of intensities between 343 and 347nm) and $[I(\infty)- I(t)]/[I(\infty)-I(0)]$ (Δ) versus time for a 1.0 wt% **CNC**/*n*-octane gel formation at 5.4 °C after being cooled from well above above T_g. The line is the best fit of the data points to a single exponential function: $Y = 1.48e^{(-x/47.4)}$, $R^2 = 0.99$.

S11
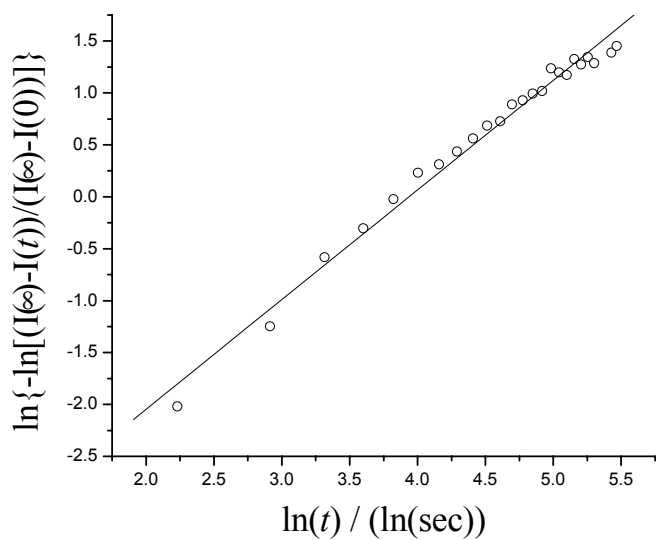
Supporting Figure 8. Plot of data from CD experiments for formation of a 1.0 wt% **CNC**/*n*-octane gel at 5.4 °C (after being cooled from well above T_g) according the log-log form of the Avrami equation. The slope $= 1.06$ ($R^2 = 0.99$).
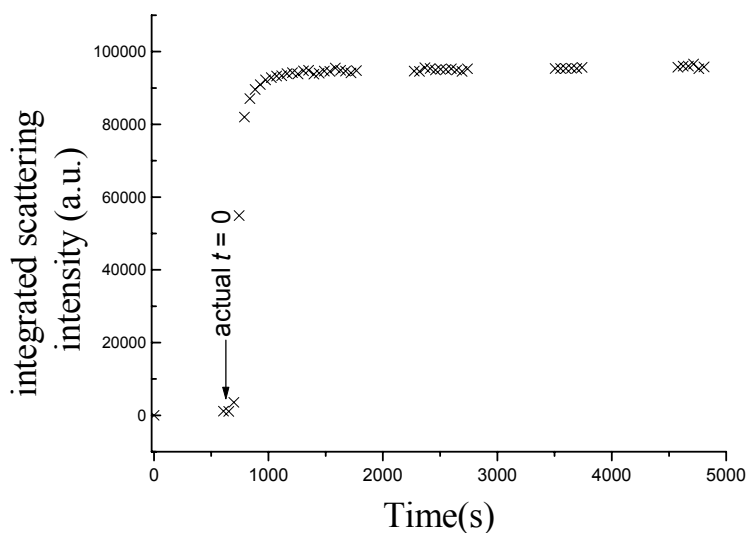

Supporting Figure 9. Time dependence of SANS intensities integrated over a 0.008-0.1 $Å^{-1}$ *q* range for a 3.0wt% **CNC**/*n*-dodecane-d_{26} sample incubated at 40 °C after being cooled from well above T_g.
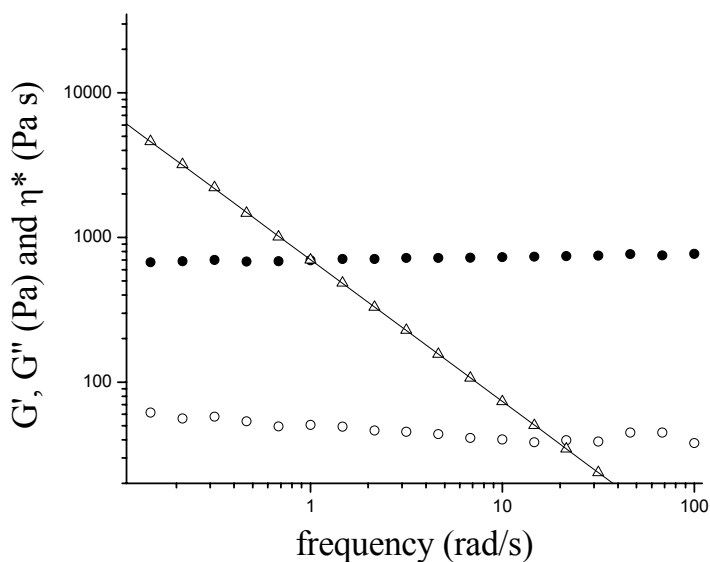
Supporting Figure 10. Dynamic rheological behavior at 25.0 °C of a 1.0 wt% **CNC**/*n*-dodecane gel prepared at 40.0 °C (1 % strain): G' (●), G" (○); η* (Δ), slope = -1.
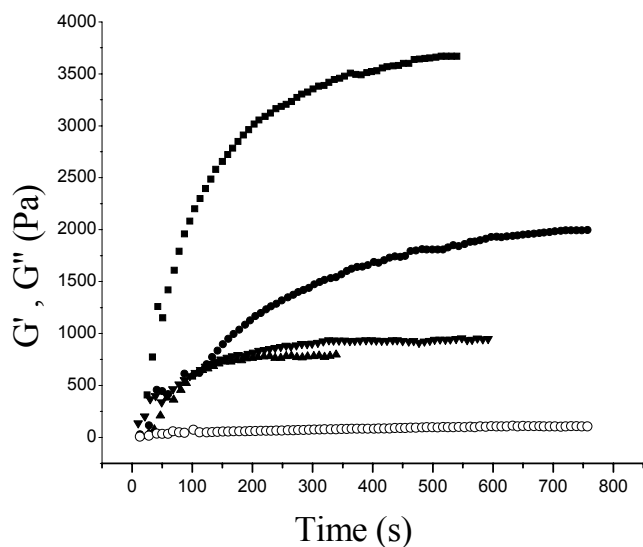

Supporting Figure 11. Plots of G' and G" versus time for a 1.0 wt% **CNC**/*n*-dodecane sample that was incubated at 0 (G', ▼), 5 (G', ▲), 10 (G' ●, G"○), and 15 °C (G', ■) after being cooled from well above T_g; 10 rad/s, 1% strain. Mechanical properties were measured at each equilibrated temperature.
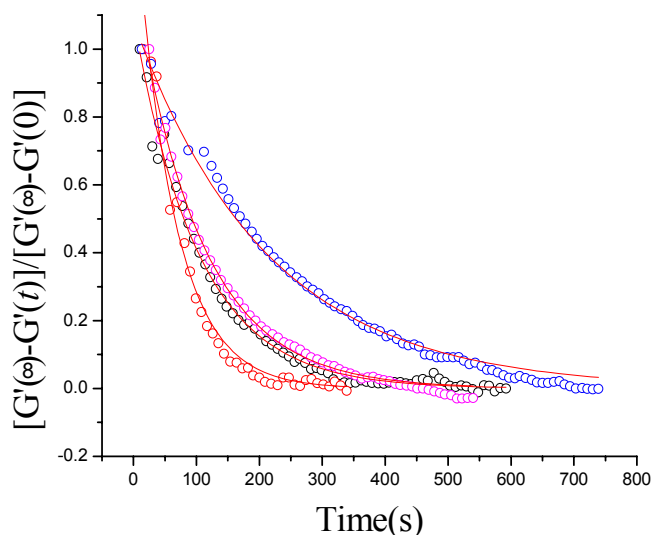
Supporting Figure 12. Plots of $[G'(\infty)- G'(t)]/[G'(\infty)-G'(0)]$ for a 1.0 wt% **CNC** in *n*-dodecane.sample versus time and their single-exponential decay fits to the Avrami equation (solid lines) from kinetic rheology data at 0, 5, 10 and 15 °C after the sample was cooled from well above T_g. Data Fits: $Y = 1.09e^{-x}/102.3$, $R^2 = 0.99$ at 0 °C (○); $Y=1.47e^{-x/60.7}$, $R^2 = 0.99$ at 5 °C (○); $Y=1.21e^{-x/211.5}$, $R^2 = 0.99$ at 10 °C (○); $Y=1.08e^{-x/105.5}$, $R^2 = 0.99$ at 15 °C (○).
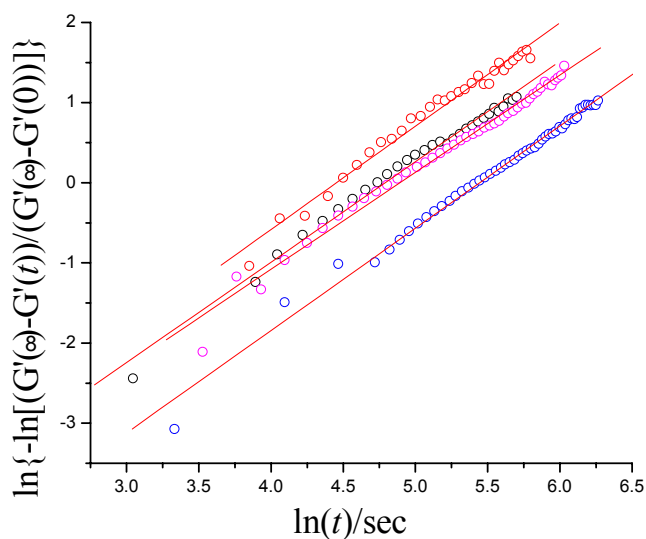

Supporting Figure 13. Linear Avrami fits of G' from kinetic rheology data for a 1.0 wt% **CNC** in *n*-dodecane sample incubated at 0, 5, 10 and 15 °C after being cooled from well above T_g. Data Fits: slope = 1.21 ($R^2 = 1.00$) at 0 °C (○); slope = 1.29 ($R^2 = 0.99$) at 5 °C (○); slope = 1.28 ($R^2 = 0.99$) at 10 °C (○); slope = 1.21 ($R^2 = 0.99$) at 15 °C (○).
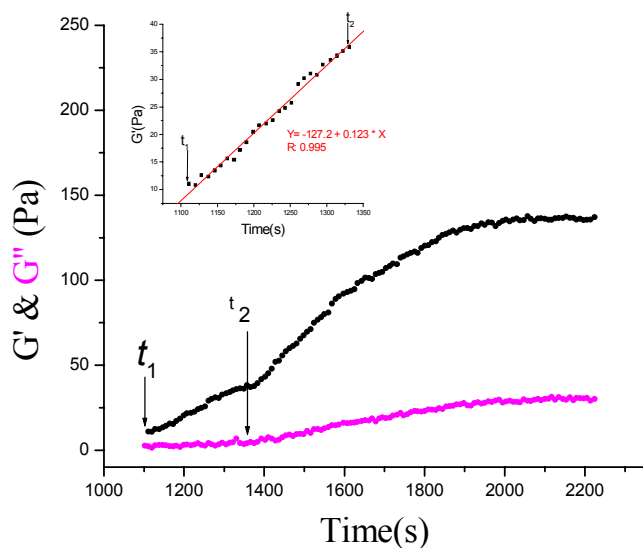
Supporting Figure 14. Dynamic rheological data (G' (●) and G" (●) recorded at 10 rad/s, 1% strain) for a 1.0 wt% **CNC**/*n*-dodecane sample undergoing gelation at 35.0 °C after being cooled from well above T_g. The inset is G' versus time during the $t_1 - t_2$ period and the best linear fit to these data; slope = 0.08 (R^2 =1.00).
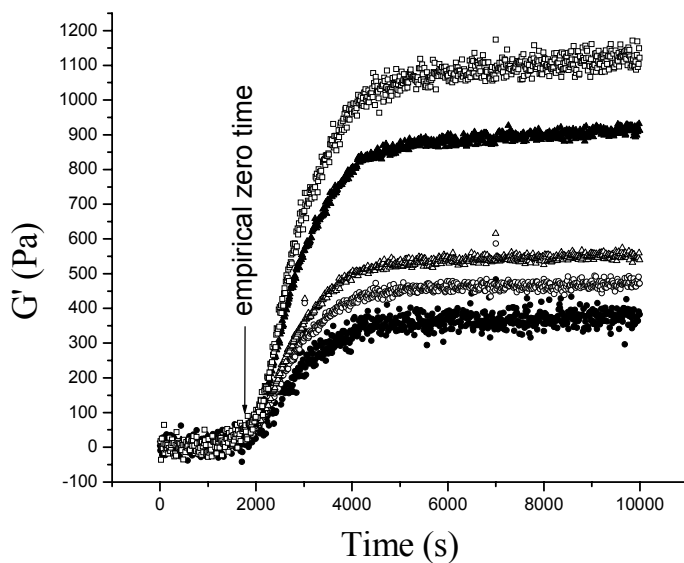
Supporting Figure 15. Elastic modulus G' as a function of time during gelation for a 1.0 wt% CNC/n-dodecane sample incubated at 40 °C. The multiple waveform rheological technique was used to simultaneously obtain data at the following frequencies: 1 (●), 5 (○), 10 (△), 50 (▲), and 100 rad/s (□).
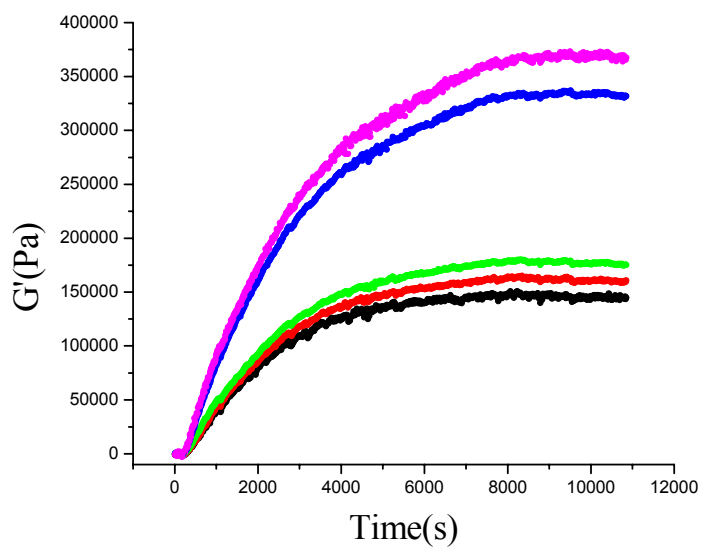
Supporting Figure 16. Elastic modulus G' as a function of time for a 1.0 wt% CNC/n-dodecane sample incubated at 35 °C after being heated above T_g. The multiple waveform rheological technique was used to simultaneously obtain data at the following frequencies: 1 Hz (black); 5 Hz (red), 10 Hz (green); 50 Hz (blue); 100 Hz (purple).

[1] Lu, L.; Cocker, M.; Bachman, R. E.; Weiss, R. G. *Langmuir* **2000**, *16*, 20-34.

[2] Eldridge, J. E.; Ferry, J. D. *J. Phys. Chem.* **1954**, *58*, 992-995.

[3] Raghavan, S. R.; Chen, L. A.; McDowell, C.; Khan, S. A. *Polymer* **1996,** *37*, 5869-5875.